Endocrine-Related Cancer (2011) **18** 143–157

Increased uptake of [^{123}I]meta-iodobenzylguanidine, [^{18}F]fluorodopamine, and [^{3}H]norepinephrine in mouse pheochromocytoma cells and tumors after treatment with the histone deacetylase inhibitors

Lucia Martiniova[1,7], Shiromi M Perera[1]*, Frederieke M Brouwers[1], Salvatore Alesci[2], Mones Abu-Asab[3], Amanda F Marvelle [1], Dale O Kiesewetter[4], David Thomasson[5], John C Morris[6], Richard Kvetnansky[7], Arthur S Tischler[8], James C Reynolds[9], Antonio Tito Fojo[10] and Karel Pacak[1]*

[1]Section on Medical Neuroendocrinology, Eunice Kennedy Shriver National Institute of Child Health and Human Development, National Institutes of Health, Building 10, Room 1E-3140, 10 Center Drive MSC-1109, Bethesda, Maryland 20892-1109, USA
[2]Clinical Neuroendocrinology Branch, National Institute of Mental Health, National Institutes of Health, Bethesda, Maryland 20892, USA
[3]Laboratory of Pathology, National Cancer Institute, National Institutes of Health, Center for Cancer Research, Bethesda, Maryland 20892, USA
[4]Intramural Science PRGMS, National Institute of Biomedical Imaging and Bioengineering, National Institutes of Health, Bethesda, Maryland 20892, USA
[5]Laboratory of Diagnostic Radiology, Warren Grant Magnuson Clinical Center, Bethesda, Maryland 20892, USA
[6]Metabolism Branch, National Cancer Institute, Center for Cancer Research, Bethesda, Maryland 20892, USA
[7]Institute of Experimental Endocrinology, Slovak Academy of Sciences, Bratislava 83306, Slovakia
[8]Department of Pathology, Tufts University School of Medicine and Tufts Medical Center, Boston, Massachusetts 02111, USA
[9]Nuclear Medicine Department, National Institutes of Health, Clinical Center, Bethesda, Maryland 20892, USA
[10]Medical Oncology Branch, National Cancer Institute, National Institutes of Health, Center for Cancer Research, Bethesda, Maryland 20892, USA

(Correspondence should be addressed to K Pacak; Email: karel@mail.nih.gov)

*(L Martiniova and S M Perera contributed equally to this work)

Abstract

[^{131}I]meta-iodobenzylguanidine ([^{131}I]MIBG) is the most commonly used treatment for metastatic pheochromocytoma and paraganglioma. It enters the chromaffin cells via the membrane norepinephrine transporter; however, its success has been modest. We studied the ability of histone deacetylase (HDAC) inhibitors to enhance [^{123}I]MIBG uptake by tumors in a mouse metastatic pheochromocytoma model. HDAC inhibitors are known to arrest growth, induce differentiation and apoptosis in various cancer cells, and further inhibit tumor growth. We report the *in vitro* and *in vivo* effects of two HDAC inhibitors, romidepsin and trichostatin A, on the uptake of [^{3}H]norepinephrine, [^{123}I]MIBG, and [^{18}F]fluorodopamine in a mouse model of metastatic pheochromocytoma. The effects of both inhibitors on norepinephrine transporter activity were assessed in mouse pheochromocytoma (MPC) cells by using the transporter-blocking agent desipramine and the vesicular-blocking agent reserpine. HDAC inhibitors increased [^{3}H] norepinephrine, [^{123}I]MIBG, and [^{18}F]fluorodopamine uptake through the norepinephrine transporter in MPC cells. *In vivo*, inhibitor treatment resulted in significantly increased uptake of [^{18}F]fluorodopamine positron emission tomography (PET) in pheochromocytoma liver metastases (19.1$\pm$3.2% injected dose per gram of tumor (%ID/g) compared to liver metastases in pretreatment scans 5.9$\pm$0.6%; $P<0.001$). Biodistribution analysis after inhibitors treatment confirmed the PET results. The uptake of [^{123}I]MIBG was significantly increased in liver

1351–0088/11/018–143
DOI: 10.1677/ERC-10-0090
Online version via http://www.endocrinology-journals.org

metastases 9.5±1.1% compared to 3.19±0.4% in untreated control liver metastases ($P<0.05$). We found that HDAC inhibitors caused an increase in the amount of norepinephrine transporter expressed in tumors. HDAC inhibitors may enhance the therapeutic efficacy of [^{131}I]MIBG treatment in patients with advanced malignant pheochromocytoma and paraganglioma.

Endocrine-Related Cancer (2011) **18** 143–157

Introduction

Up to 36% of patients diagnosed with pheochromocytoma or paraganglioma will develop metastatic disease and have a 5-year survival of ~50% (O'Riordain *et al.* 1996, Mundschenk & Lehnert 1998, John *et al.* 1999, Plouin *et al.* 2000, Lenders *et al.* 2005, Adjalle *et al.* 2009, Gaal *et al.* 2010). Moreover, patients with metastatic pheochromocytoma and paraganglioma often exhibit excessive levels of circulating catecholamines. This results in an increased risk of hypertensive complications, including stroke, myocardial infarction, and tachyarrhythmia. Current treatments for malignant pheochromocytoma or paraganglioma include targeted radiation using [^{131}I]meta-iodobenzylguanidine ([^{131}I]MIBG), cytotoxic chemotherapy, the somatostatin analog octreotide, chemoembolization, and less commonly, radiofrequency or cryoablation (Averbuch *et al.* 1988, Kopf *et al.* 1997, Loh *et al.* 1997, Sisson *et al.* 1999, Takahashi *et al.* 1999, Pacak *et al.* 2001*a*, Munver *et al.* 2003). The most common chemotherapeutic regimen used for metastatic pheochromocytoma and paraganglioma is a combination of cyclophosphamide, vincristine, and dacarbazine (CVD). A long-term follow-up study conducted on 18 patients reported a complete response rate of 11% and a partial response rate of 44% of metastatic pheochromocytoma and paraganglioma patients after CVD treatment (Huang *et al.* 2008). However, the survival rate did not differentiate between those patients treated with or without CVD chemotherapy, also described by a recent study (Huang *et al.* 2008, Nomura *et al.* 2009).

Among current therapeutic options for metastatic pheochromocytoma and paraganglioma, [^{131}I]MIBG is still the most effective therapy because it specifically targets tumor cells via the membrane norepinephrine transporter system (Sisson & Wieland 1986, Sisson *et al.* 1987, Glowniak *et al.* 1993, Rose *et al.* 2003, Gonias *et al.* 2009, Shilkrut *et al.* 2010), expressed in most lesions. Uptake of [^{131}I]MIBG results in accumulation of [^{131}I] in tumor cells and their destruction by high-energy β-irradiation. Unfortunately, only about 30% of patients show a response to [^{131}I]MIBG, and cure is extremely rare (Loh *et al.* 1997). This disappointing response rate is likely related to reduced expression of the norepinephrine transporter and the number of catecholamine storage granules in metastatic tumor that results in suboptimal [^{131}I]MIBG concentrations within the tumor cells. Furthermore, the low-specific activity of most preparations of [^{131}I]MIBG causes a low accumulation of radioactivity in pheochromocytoma due to significant competitive uptake with unlabeled MIBG. In addition, elevated circulating catecholamines in these patients compete with [^{131}I]MIBG for transporter-mediated uptake by the tumor cells, further reducing uptake of the therapeutic agent (Eldadah *et al.* 2004). Finally, proper function of vesicular uptake is also important, which is well supported by the work of Kolby *et al.* (2003), indicating the importance of secretory granules containing vesicular monoamine transporters for the uptake and retention of [$^{123/131}$I]MIBG.

A number of histone deacetylase (HDAC) inhibitors have demonstrated activity as anticancer agents. Romidepsin (depsipeptide, FR901228), a complex cyclic peptide isolated from *Chromobacterium violaceum*, has demonstrated potent antitumor activity *in vitro* and against human tumor xenografts (Marks *et al.* 2000) and in murine tumors *in vivo* (Ueda *et al.* 1994*a*,*b*). Laboratory studies have demonstrated that romidepsin, similar to other HDAC inhibitors, induces expression of a specific subset of genes involved in cell growth inhibition and induction of differentiation (Van Lint *et al.* 1996). Romidepsin is able to cause both a p21-dependent G1 and p21-independent G2 arrest, with the G2 arrest appearing more cytotoxic than the G1 arrest (Sandor *et al.* 2000*a*,*b*).

By extension, HDAC inhibitors might also benefit the treatment of metastatic pheochromocytoma and paraganglioma by virtue of their ability to induce growth inhibition and/or apoptosis in pheochromocytoma cells, increase the entry and retention of radioisotopes (e.g. [^{131}I]MIBG), and stimulate the differentiation of malignant pheochromocytoma and paraganglioma cells with partial or total restoration of the phenotypic traits of the normal chromaffin cell (Li *et al.* 2002). From previous work we learned that romidepsin was able to differentiate thyroid cancer cells and to increase the entry of ^{131}I into these cells in patients with negative ^{131}I scan (Kitazono *et al.* 2001, Furuya *et al.* 2004). We also learned that HDAC

inhibitors were able to increase the efficacy of cisplatin, a compound that is known to increase the expression of norepinephrine transporters (Kim *et al*. 2003, Cleary & Phillips 2006). HDAC inhibitors are also known to enhance a cocaine-induced antidepressant effect of stress (Kumar *et al*. 2005). All these effects and unpublished preliminary findings of the NIH investigators suggested that HDAC inhibitors could potentially affect norepinephrine transporters in chromaffin or neuronal cells, which led us to hypothesize that HDAC inhibitors might increase the expression of norepinephrine transporters and thus increase the entry of [^{131}I]MIBG into pheochromocytoma cells.

In this study, we examined the effects of two unrelated HDAC inhibitors, romidepsin and trichostatin A, in mouse pheochromocytoma (MPC) cells *in vitro* and a MPC mouse model of metastatic pheochromocytoma (Ohta *et al*. 2008, Martiniova *et al*. 2009*b*). We examined the effects of HDAC inhibition on cell proliferation, uptake of [^{3}H]norepinephrine, [^{123}I]MIBG, [^{18}F]fluorodopamine, and norepinephrine transporter expression in MPC cells. We also assessed the effect of a single dose of romidepsin on [^{18}F]fluorodopamine uptake by pheochromocytoma liver metastases and demonstrated the effect of trichostatin A on [^{123}I]MIBG uptake by liver lesions in a mouse model of metastatic pheochromocytoma.

Materials and methods

Reagents

RPMI 1640, DMEM, trypsin–EDTA, penicillin/streptomycin 100×, and 1 M HEPES buffer were purchased from Invitrogen-Life Technologies. Fetal bovine serum (FBS) and donor horse serum (DHS) were obtained from Gemini Bio-Products (Woodland, CA, USA). L-2, 5, 6-^{3}H-norepinephrine was purchased from NEN Life Science Products (Boston, MA, USA). BSA, dimethyl sulfoxide, and all the components of the Krebs Ringer Glucose (H-KRG) buffer were purchased from Sigma Chemical Co. PBS was obtained from Biosource International (Camarillo, CA, USA), and Triton X-100 was obtained from Fisher Scientific (Suwanee, GA, USA). Romidepsin was kindly provided by the Developmental Therapeutics Program, National Cancer Institute (Bethesda, MD, USA). Trichostatin A was purchased from Sigma Chemical Co.

Cell culture

MPC cells (cell line 4/30/PRR) were established from heterozygous neurofibromatosis knockout mice (Powers *et al*. 2000). Cells were cultured in RPMI 1640 supplemented with 10% DHS, 5% FBS with penicillin/streptomycin, and maintained at 37 °C in 5% CO_2. Cells from passages 26–38 were used in the experiments.

Cell proliferation assay

The cytotoxic effects of romidepsin and trichostatin A were examined using the XTT-assay (Cell Proliferation kit II, Roche Applied Science). MPC cells were seeded into 96-well flat-bottomed plates at 50 000 cells/well and incubated with increasing concentrations of romidepsin or trichostatin A diluted in medium at 37 °C for 48 or 72 h. The XTT mixture was then added, and the cells were incubated for 18 h. After incubation, the absorbance at 690 nm was measured using a microplate reader (Bio-Rad Laboratories). All experiments were performed in octuplicate.

Uptake of [^{3}H]norepinephrine

The uptake of norepinephrine by MPC cells was determined using [^{3}H]norepinephrine and following a modification of the protocol described by Jaques *et al*. (1984). MPC cells (100 000 cells/well) in 24-well plates were incubated with increasing concentrations of romidepsin from 0.001 to 10 ng/ml or trichostatin A at 6.25–100 ng/ml diluted in the medium for 48 or 72 h at 37 °C. After treatment, cells were washed three times with 0.5 ml H-KRG buffer (H-KRG: 125 mM NaCl, 4.8 mM KCl, 2.6 mM $CaCl_2$, 1.2 mM $MgSO_4$, 5.6 mM glucose, 25 mM HEPES, 1 mM ascorbic acid, pH 7.35), followed by a 10 min preincubation in H-KRG buffer (0.5 ml/well) at 37 °C. Next, [^{3}H]norepinephrine (25 nM/well) was added and the cells were incubated at 37 °C for 10 min. [^{3}H]norepinephrine uptake was stopped by rapidly chilling the plates on ice, and the cells were washed twice with 0.1% albumin in PBS at 4 °C. Cells were lysed with 0.5 ml Triton-X100 (0.1%) and aliquots of the cell lysates were transferred into scintillation vials. After addition of the Biosafe-II scintillation cocktail (Research Products International, Mount Prospect, IL, USA), cell-associated β radiation was counted in a β-counter (Beckman Coulter LS 60000 IC).

Uptake of [^{123}I]MIBG and [^{18}F]fluorodopamine

The [^{123}I]MIBG and [^{18}F]fluorodopamine uptake studies, the treatment of the cells, the washing steps, and the incubations were performed following the same protocol used for the [^{3}H]norepinephrine uptake assay. MPC cells were incubated with 0.5 ng/ml romidepsin

or 12.5 ng/ml trichostatin A for 48 or 72 h at 37 °C. [^{123}I]MIBG 0.6–0.7 μCi/ml (22.2–25.9 kBq), specific activity of 2 mCi/0.08 mg (74 MBq/0.08 mg), and [^{18}F]fluorodopamine 0.6–0.7 μCi/ml (22.2–25.9 kBq), specific activity of 20 mCi/3.23 mg (740 MBq/3.23 mg) or 17.31 mCi/2.49 mg (640.47 MBq/2.49 mg), were added to the plates, which were incubated at 37 °C for 10 min to asses uptake and 120 min to assess accumulation in cells. After incubation, [^{123}I]MIBG uptake was stopped by rapidly chilling the plates on ice, and the cells were washed twice with 0.1% albumin in PBS at 4 °C. The incubation medium was collected, and the cells were washed with cold PBS, trypsinized, and the cell-associated radioactivity was measured using a γ-counter (1480 Wizard 3, Automatic Gamma Counter, PerkinElmer, Waltham, MA, USA).

In a subset of experiments, uptake studies with romidepsin and trichostatin A treatment were carried out in the presence or absence of 1 μM desipramine to block catecholamine uptake (Lingen *et al*. 1994), or 10 μM reserpine to block vesicular catecholamine translocation (Eisenhofer *et al*. 1989, Cornelissen *et al*. 1997). All experiments were performed in quadruplicate.

Protein collection and analysis

For these experiments, cells were incubated in 25 ml flasks with 0, 0.25, 0.5, or 0.75 ng/ml of romidepsin or 0, 6.25, 12.5, or 25 ng/ml of trichostatin A for 72 h. After two washes with PBS, cells were pelleted and lysed. Cell lysates were added to the loading buffer (1:1 GTC/PBS, Invitrogen/Cellgro). The samples were serially diluted 1:2 and loaded into a 96-well vacuum manifold (Bio-Rad) with two sheets Protran membrane (Schleicher & Schuell, Keene, NH, USA), and a vacuum was slowly applied. The membrane was removed and washed twice in TBS before being probed for GAPDH at 1:500 (American Research Products, Belmont, MA, USA). After antibody binding, the membrane was washed three times in TTBS. The blot was then incubated with HRP-linked anti-mouse Ig whole antibody at 1:1000 (Amersham) and imaged using ECL western blotting kit (Amersham). Next, the membrane was stripped using Re-Blot Plus Mild (Chemicon, Temecula, CA, USA) for 10 min. Subsequently, it was probed for anti-acetyl histone H3 1:2200 and again washed three times in TTBS, followed by HRP-linked anti-rabbit Ig whole antibody at 1:1000 (Amersham) and imaged as before. Densitometry was performed on films using the IPLab gel software.

Ultrastructural studies

The effect of treatment with either 0.5 ng/ml romidepsin or 12.5 ng/ml trichostatin A on MPC cell morphology and ultrastructure was examined by transmission electron microscopy. After three washes with PBS, cells were double-fixed in PBS-buffered glutaraldehyde (2.5%) and osmium tetroxide (0.5%), dehydrated, embedded into Spurr's epoxy resin, and coded to ensure unbiased assessment. Ultra thin sections (90 nm) were made and double-stained with uranyl acetate and lead citrate and viewed in a Philips CM10 transmission electron microscope.

Animal model

The metastatic MPC model used in this study was previously described (Martiniova *et al*. 2009*a*,*b*). Briefly, female 6–8-week-old (20–22 g) athymic nude mice (NCr-nu; Taconic, Germantown, NY, USA) were injected through the tail vein with 1×10^6 MPC (MPC 4/30 PRR) cells. MPC cells were mixed with 100 μl PBS and held at room temperature prior to injection. Mice were anesthetized using isoflurane/O_2 (1.5–5% v/v) before all imaging and treatment procedures. All animal studies were conducted according to the National Institutes of Health Guide for the Care and Use of Animals under an approved protocol from the Institutional Animal Care and Use Committee.

In vivo magnetic resonance imaging

Magnetic resonance images were obtained with a 3T magnetic resonance imaging (MRI) scanner (Intera, Philips Medical System, Best, The Netherlands) using a dedicated 40 mm inner diameter solenoid coil (Philips). Localization and monitoring of liver lesions were carried out as previously described (Martiniova *et al*. 2009*a*). Briefly, with anesthetized animals in the prone position, respiratory-triggered T_2-weighted spectra were acquired with the following parameters: FOV $8.0\times8.0\times2.0$ cm^3, data matrix 512×512, 40 slices, TE/TR 65/4500 ms, flip angle 90°, slice thickness 0.5 mm, 0.156×0.156 mm^2 in-plane resolution, scan time of 5–7 min for two signal averages depending on the respiratory rate. No contrast agent was used for MRI. Animals were scanned 4–5 weeks after the injection of MPC cells to determine the liver tumor size.

[^{123}I]MIBG and [^{18}F]fluorodopamine biodistribution studies

HDAC inhibitors treatment was carried out using the protocol described by Goldsmith *et al*. (2007) with a slight modification. Briefly, mice were treated with

romidepsin at a dose of 3.6 mg/kg; however, mice with extensive liver metastases did not tolerate this dose. Thus, a single lower dose of romidepsin, 2.5 mg/kg, was used to evaluate its effect on isotope accumulation in the tumors. The same concentration was used for trichostatin A. Both romidepsin and trichostatin A were diluted in saline and intravenously administered by injection of 150 µl at a rate of 10 µl/min. [^{123}I]MIBG and [^{18}F]fluorodopamine biodistribution studies began 24 h after drug administration.

For [^{123}I]MIBG biodistribution studies, anesthetized mice ($n=3$) were injected through the lateral tail vein with 150 µl normal saline containing 2.5 mg/kg trichostatin A. Trichostatin A was injected 24 and 2 h before the administration of 25–27 µCi (925–999 kBq) [^{123}I]MIBG. Untreated control mice ($n=4$) were injected with a volume of 150 µl vehicle diluted in saline and studied at the same time points with the same dose of [^{123}I]MIBG. Both the groups were killed by cervical dislocation 120 min post injection of [^{123}I]MIBG. Samples of the liver metastases and normal liver were collected and weighed.

For [^{18}F]fluorodopamine biodistribution studies, a single dose of 2.5 mg/kg romidepsin was injected into mice ($n=7$) 24 h before administration of 50–60 µCi (1850–2220 kBq) [^{18}F]fluorodopamine. Control mice ($n=7$) received the same dose of [^{18}F]fluorodopamine. Both the groups were killed 60 min post injection. Samples of the liver lesions and normal liver were collected and weighed. The concentrations of [^{123}I]MIBG and [^{18}F]fluorodopamine in the liver tumors and normal liver tissue were assayed using an automatic γ-counter (Model 1480 Wallac Wizard, PerkinElmer, Shelton, CT, USA). Standards of 1:10 of the injected dose were prepared and counted along with all samples. Background counts were subtracted from the reported ^{123}I and ^{18}F counts per minute. The injected counts were determined from the standard counts and the quantitative data, expressed as percentage of injected dose per gram (%ID/g), were determined as previously described (Toyama *et al*. 2004).

[^{18}F]fluorodopamine positron emission tomography imaging

Tumors were monitored using positron emission tomography (PET) imaging. The procedure for romidepsin pretreatment evaluation consisted of two PET scans, where mice were injected with 50–60 µCi (1850–2220 kBq) [^{18}F]fluorodopamine, performed on the same mice. Mice were treated with a single dose of 2.5 mg/kg romidepsin ($n=4$). The first scan was performed before the treatment as a baseline measurement. One week later, a second scan 24 h after treatment with romidepsin was performed on the same mice.

PET scans were performed using the Advanced Technology Laboratory Animal Scanner (ATLAS; Seidel 2003), which has a transverse field-of-view (FOV) of 6.8 cm and an axial FOV of 2 cm. PET images were reconstructed by a 2D-ordered-subset expectation maximization (2D OSEM) algorithm (5 iterations and 16 subsets), achieving a 1.5 mm full width at half maximum (FWHM) resolution at the center (Toyama *et al*. 2004). The reconstructed voxel size was $0.56\times0.56\times1.125$ mm^3. No correction was applied for attenuation or scatter. Dynamic data acquisition determining the pharmacokinetics of [^{18}F]fluorodopamine in liver tumors and liver parenchyma started about 1 min after injection. Scanning parameters were set for one frame/10 min, up to six frames. Whole body data acquisitions (two bed positions, each 10 min) started consecutively after the dynamic acquisition. Whole body acquisitions (achieving 2×2 cm $=4$ cm of the field of view), including images of the lungs through the kidneys, were acquired after administration of 50–60 µCi (1850–2220 kBq) [^{18}F]fluorodopamine.

If liver tumors are smaller (in any dimension) than ~2.5 times the FWHM of the spatial resolution of the PET scanner, a distortion called a partial volume effect occurs (Hutchins *et al*. 2008). Therefore, liver lesions were analyzed only if they were larger than 4 mm in diameter as obtained by MRI. This is the minimum size required to exclude partial volume effects in small animal PET when monitoring lesions for potential physiological changes (Keyes 1995). The [^{18}F] activity concentration of the radionuclide was expressed as the tumor-to-liver ratio (TLR), which was obtained by comparing uptake in the liver lesions with that in the liver parenchyma. PET results are also expressed as standardized uptake value (SUV), which was determined as described previously (Green *et al*. 2001).

SYBR Green real-time PCR for quantification of norepinephrine transporter expression in liver tumors

Norepinephrine transporter expression was quantified by quantitative real-time PCR. Total RNA was extracted from isolated liver metastases of untreated control mice and from trichostatin A-treated mice using the RNeasy Midi kit (Qiagen) according to the manufacturer's instructions. After reverse transcribing mRNA, real-time PCR was performed in triplicate

using the SYBR Green PCR Master Mix (Applied Biosystems, Foster City, CA, USA) in a 7500 Real-time PCR system (Applied Biosystems) as previously described (Ichijo *et al*. 2005). Use of forward primer 5′-AGAGCAGTGGGATCCATGAC-3′ and reverse primer 5′-CCAGGAGCACAAACAAGACA-3′ yielded a 168 bp product. Obtained threshold cycle (C_T) values of the norepinephrine transporter gene in liver lesion samples after trichostatin A treatment ($n=7$) were normalized to those of β-actin, and their relative mRNA expression was expressed as fold induction over the baseline of untreated controlliver lesions ($n=6$). The dissociation curves of the primer pairs showed a single peak, and PCR produced a single expected DNA band in an agarose gel analysis. Statistical analyses were carried out by unpaired *t*-test with the two-tailed *P* value.

Data analyses

Results are presented as the mean±S.E.M. from a minimum of three experiments. Before performing any statistical test, all data were tested for normal distribution and equal variance. Statistical differences between groups of data were assessed by ANOVA, followed by the Student–Neuman–Keuls test for group comparison. The level of statistical significance was set at $P<0.05$.

Results

Romidepsin and trichostatin A demonstrated a dose- and time-dependent inhibition of MPC cell proliferation

Treatment with romidepsin or trichostatin A both induced a dose-dependent decrease in MPC cell proliferation. Growth inhibition curves after 48 and 72 h of exposure to either drug are shown in Fig. 1A and B. After a 72 h exposure, the 50% inhibitory concentrations (IC_{50}) were determined to be 1.56 ng/ml for romidepsin and 50 ng/ml for trichostatin A.

Romidepsin and trichostatin A increased [^{3}H]norepinephrine-specific uptake in MPC cells

A significant dose- and time-dependent increase in the [^{3}H]norepinephrine-specific uptake was observed in MPC cells treated with romidepsin at concentrations of 0.25–0.5 ng/ml, and trichostatin A concentrations of 6.25–12.5 ng/ml. This increase was followed by a decreased uptake at the highest concentrations of both tested drugs (Fig. 1C and D). The maximal increase in

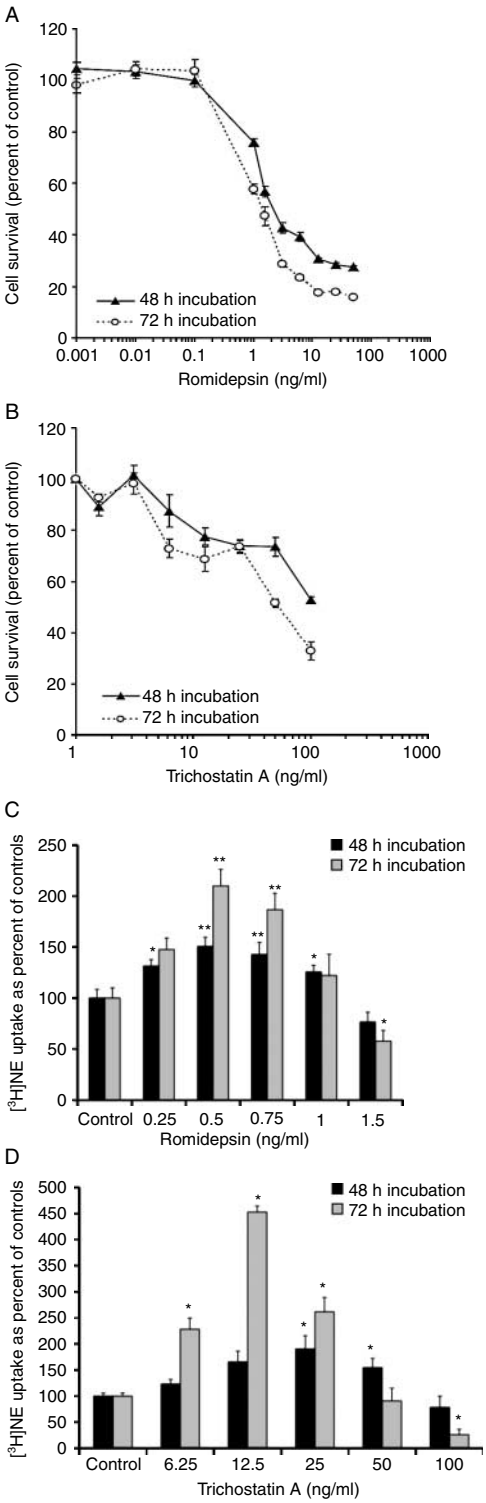

Figure 1 (A) Romidepsin and (B) trichostatin A demonstrated a dose- and time-dependent effect on MPC cell growth. Results are presented as mean±S.E.M. Increased [^{3}H]norepinephrine ([^{3}H]NE) uptake in MPC cells after treatment with romidepsin (C) and trichostatin A (D) (*$P<0.05$; **$P<0.005$, compared to control, untreated cells).

[^{3}H]norepinephrine uptake occurred in MPC cells after 72 h of treatment with 0.5 ng/ml of romidepsin and 12.5 ng/ml of trichostatin A. In subsequent experiments, concentrations of 0.5 ng/ml romidepsin and 12.5 ng/ml trichostatin A were used.

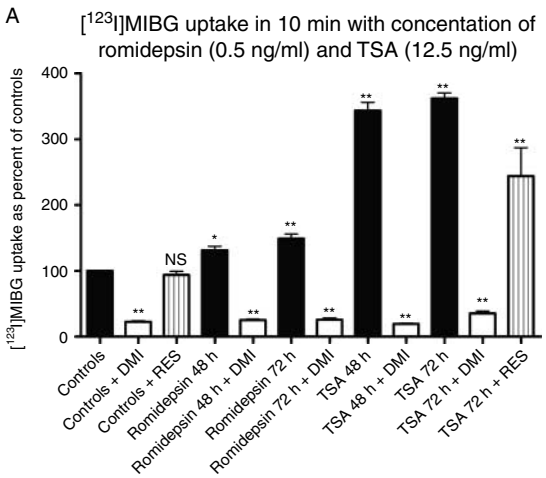

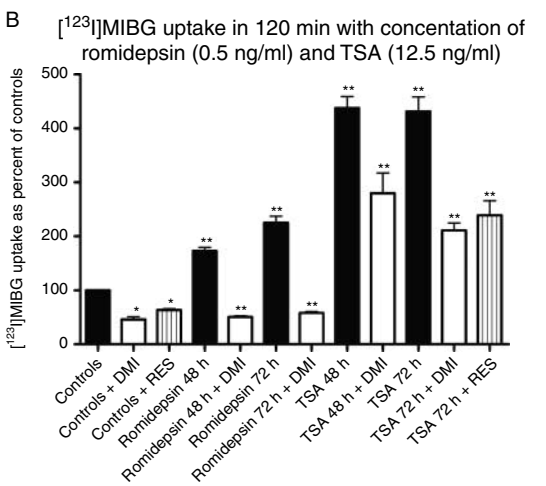

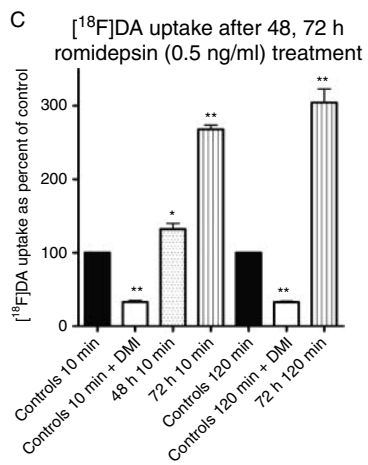

Romidepsin or trichostatin A increased [^{123}I]MIBG and [^{18}F]fluorodopamine uptake in MPC cells

The maximal amount of [^{123}I]MIBG uptake in MPC cells occurred 72 h after treatment with 0.5 ng/ml romidepsin in both short-term (Fig. 2A) and long-term (Fig. 2B) culture. Trichostatin A (12.5 ng/ml) resulted in approximately the same levels of [^{123}I]MIBG uptake after 48 h as after 72 h (Fig. 2A and B). The uptake of [^{123}I]MIBG in MPC cells was ~3.6-fold higher than in the control group at 10 min, and 4.4-fold higher at 120 min after 72 h treatment with trichostatin A. Similarly, for romidepsin, the uptake of [^{123}I]MIBG was ~1.5 times that in the control group at 10 min, and 2.2 times higher at 120 min.

In order to find out whether the increase in [^{123}I]MIBG uptake was due to inhibition of transport across the cell membrane or impaired granule storage, we examined the effect of desipramine on [^{123}I]MIBG uptake and retention, and also the effect of reserpine on storage of [^{123}I]MIBG in vesicles. Desipramine inhibited the entry of [^{123}I]MIBG into both untreated and treated MPC cells; the inhibitory effect was more pronounced at 10 min than at 120 min (Fig. 2A and B). A similar, though less pronounced, inhibitory effect was observed with reserpine at 120 min in untreated cells, and at 10 and 120 min in cells treated with trichostatin A (Fig. 2A and B). Similarly, increased accumulation of [^{18}F]fluorodopamine was observed in MPC cells after treatment with romidepsin for 48 and 72 h (Fig. 2C). Desipramine significantly inhibited the entry of [^{18}F]fluorodopamine into MPC cells (Fig. 2C).

Romidepsin or trichostatin A treatment increased acetylation of histone H3

Blot analysis showed increased acetylation of histone H3 in MPC cells at the same doses of romidepsin or trichostatin A that had been demonstrated to decrease

Figure 2 Treatment with romidepsin or trichostatin A increased [^{123}I]MIBG uptake in MPC cells. (A) The effect of the norepinephrine transporter blockers, desipramine (DMI) and reserpine (RES), on 10 min of uptake time of [^{123}I]MIBG after 48 and 72 h of treatment with romidepsin and trichostatin A. Data are shown as percentage of [^{123}I]MIBG uptake in untreated control cells (baseline). (B) Effect of desipramine (DMI) or reserpine (RES) on 120 min of uptake time of [^{123}I]MIBG after 48 and 72 h of treatment with romidepsin and trichostatin A. (C) The uptake of [^{18}F]fluorodopamine ([^{18}F]DA) in MPC cells in 10 and 120 min. The effect on [^{18}F]DA uptake was studied after 48 and 72 h of romidepsin treatment, and the association of specific transporters with uptake of [^{18}F]DA was confirmed with desipramine (DMI). Desipramine or reserpine was added 30 min prior to [^{123}I]MIBG and [^{18}F]DA dosing. Results are presented as mean±S.E.M. (NS, not significant, $*P<0.05$; $**P<0.005$).

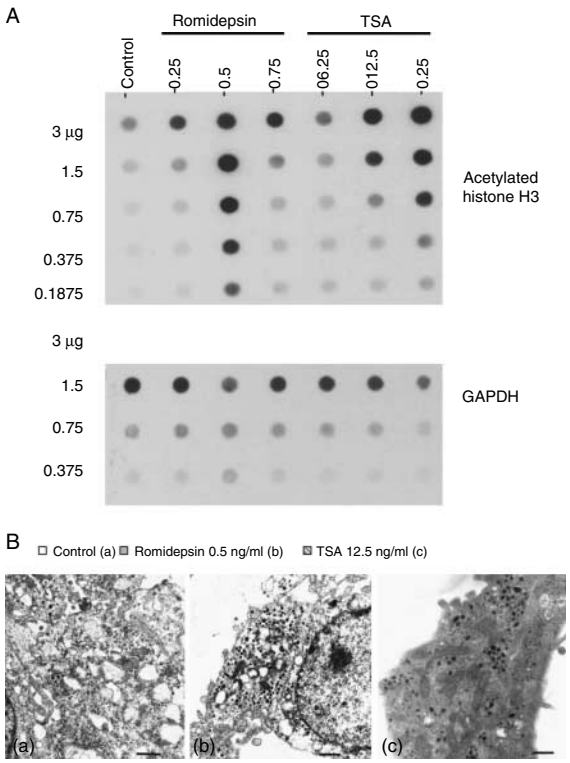

Figure 3 (A) Levels of acetylated histone H3 at various concentrations of romidepsin or trichostatin A by dot blot analysis. GAPDH was used as a loading control. (B) EM photomicrographs of MPC cells showing the presence of granules in treated cells: (a) untreated cells, (b) romidepsin 0.5 ng/ml, (c) trichostatin A 12.5 ng/ml. Bar = 1 μM.

cell proliferation and increase [^{3}H]norepinephrine and [^{123}I]MIBG uptake (Fig. 3A). Neurosecretory granules were present, but no differences were noted between control and treated cells (Fig. 3B).

MRI imaging

MRI detected multiple liver lesions in our *in vivo* model. Liver lesions ≥4 mm in diameter were present 5 weeks after tail vein injection of MPC cells and were suitable for PET imaging. Moreover, we were able to determine the growth of individual lesions and correlate radionuclide uptake with the size of the lesions.

Trichostatin A and romidepsin increased [^{18}F]fluorodopamine and [^{123}I]MIBG uptake in metastatic pheochromocytomas

Tumor-bearing mice were killed 120 min post [^{123}I]MIBG injection, and liver metastases of various sizes (2 mm to >8 mm diameter) were dissected free to examine the relationship between tumor size and [^{123}I]MIBG uptake. The average concentration of [^{123}I]MIBG in all liver metastases after trichostatin A treatment was 9.5±1.1% compared with 3.19±0.4% in untreated control liver metastases ($P<0.05$). The corresponding TLR values were 3.17 after treatment with trichostatin A and 1.86 in the untreated control mice. Similar results were observed for [^{18}F]fluorodopamine biodistribution. Mice treated with romidepsin demonstrated values of 18.3±1.35 vs 4.7±0.6% ($P<0.001$), and the TLR value was significantly higher in the treated group, 4.95 vs 1.49. No relationship was observed between the tumor size and uptake of either [^{18}F]fluorodopamine or [^{123}I]MIBG in both the control and HDAC inhibitor-treated groups (Fig. 4).

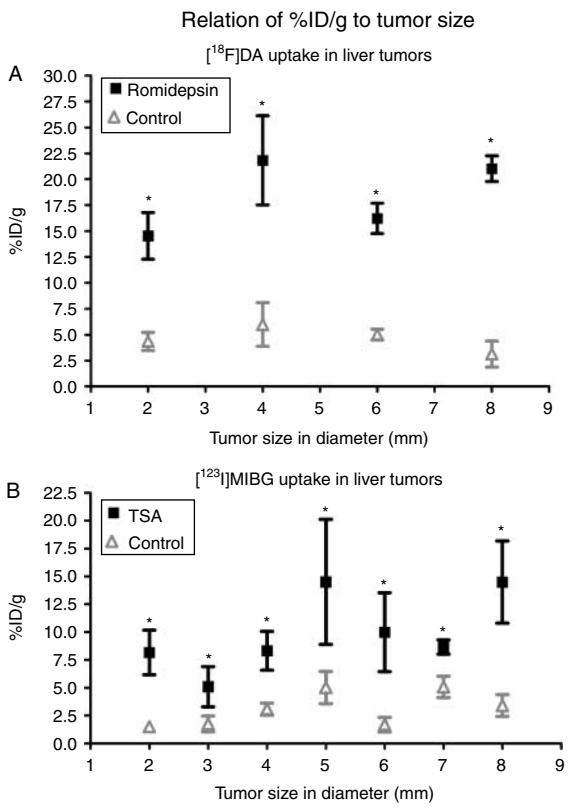

Figure 4 Summary of biodistribution of both tracers after romidepsin or trichostatin A treatment. The biodistribution of (A) [^{18}F]fluorodopamine ([^{18}F]DA) or (B) [^{123}I]MIBG has no relationship to tumor size in either the control or the treated groups. [^{18}F]DA uptake was evaluated from 14 control liver tumor samples and 15 treated liver tumor samples. [^{123}I]MIBG uptake was evaluated from 30 control tumor samples and 29 treated tumor samples. Every tumor size is derived from the mean±S.E.M. of at least three tumor samples. Increased uptake of [^{123}I]MIBG was significant in liver metastases after treatment compared to uptake in control liver lesions (*$P<0.05$).

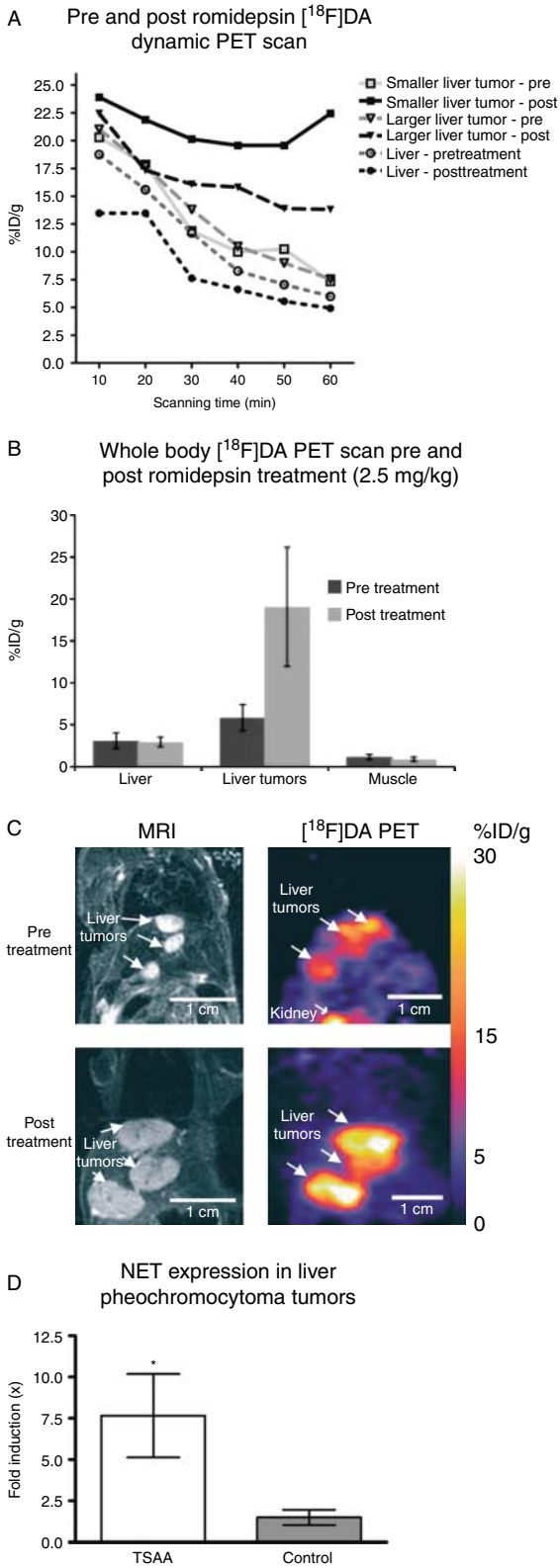

Increased [^{18}F]fluorodopamine PET uptake in metastatic pheochromocytoma lesions in mice treated with romidepsin

The effect of romidepsin was evaluated by serial PET imaging. MRI measured the size of liver lesions 1 day before [^{18}F]fluorodopamine PET imaging both pre- and post-romidepsin treatment. Representative dynamic PET images, acquired over 60 min after injection of [^{18}F]fluorodopamine, showed increased radionuclide accumulation in posttreatment scans compared to pretreatment scans of large and small tumors (Fig. 5A). Whole body PET images confirmed the increased accumulation of [^{18}F]fluorodopamine in pheochromocytoma liver metastases after romidepsin treatment compared with the baseline scan. Uptake of [^{18}F]fluorodopamine was significantly higher in liver lesions after romidepsin treatment (%ID/g: 19.1 $\pm$3.2%; SUV_{max}: 3.8 $\pm$ 1.4 respectively) compared to liver lesions in pretreatment scans (%ID/g: 5.9 $\pm$ 0.6%; SUV_{max}: 1.26 $\pm$ 0.36, $P<0.001$; Fig. 5B). TLR values were 1.62 for pretreatment and 5.56 for posttreatment. These results were consistent with the increased [^{18}F]fluorodopamine concentration detected in liver lesions. Representative pretreatment and posttreatment PET/MRI images of the same mouse are presented in Fig. 5C. The color scale indicates the %ID/g uptake values in the PET images.

Increased norepinephrine transporter mRNA in liver tumors treated with trichostatin A

Quantitative RT-PCR demonstrated a significant increase in the expression of the norepinephrine transporter in the liver metastases of mice treated with trichostatin A in comparison to untreated animals (Fig. 5D).

Figure 5 (A) Dynamic PET acquisition imaging captured the pharmacokinetics of [^{18}F]fluorodopamine ([^{18}F]DA) in liver tumors and in the liver, pretreatment and posttreatment, using a 60 min imaging period. (B) PET imaging showing [^{18}F]DA as a percentage of injected dose per gram (%ID/g) uptake (mean $\pm$S.D.) 6 days before and 24 h after treatment with a single i.v. dose of romidepsin (2.5 mg/kg) in the liver, pheochromocytoma liver metastases, and muscle. [^{18}F]DA uptake in the metastatic liver lesions is significantly increased after administration of romidepsin compared to the uptake in the same lesions 1 week earlier on the pretreatment scan ($P<0.001$). (C) Representative pretreatment and posttreatment PET/MRI images of the same mouse. There was 1 week between pretreatment and posttreatment scans. Tumor growth over that 1 week is presented in MRI (left panels) and the corresponding PET of [^{18}F]DA uptake (right panel) was imaged 24 h after MRI. (D) Relative mRNA expression of the norepinephrine transporter (NET) in the liver lesion samples after trichostatin A treatment ($n=7$) is higher than in control, untreated liver lesions ($n=6$). RNA concentrations were normalized for β-actin; (*$P<0.05$).

Discussion

Treatment with the HDAC inhibitors romidepsin and trichostatin A increased [^{123}I]MIBG, [^{18}F]fluorodopamine, and [^{3}H]norepinephrine uptake in MPC cells *in vitro* and *in vivo* in liver metastatic lesions through the upregulation of the cell membrane norepinephrine transporter system. These data support the notion that this approach may be used clinically to augment the therapeutic efficacy of [^{131}I]MIBG in patients with advanced malignant pheochromocytoma, paraganglioma, and other related tumors such as neuroblastoma.

A number of HDAC inhibitors induce growth arrest, differentiation, and/or apoptosis in various tumor cell lines and *in vivo* (Marks *et al*. 2001). Voronistat (Zolinz[a], Patheon, Inc., Mississauga, ON, Canada) and romidepsin (Istodax, Celgene, Summit, NJ, USA) are now approved for the treatment of cutaneous T-cell lymphoma as single agents (Mann *et al*. 2007, Piekarz *et al*. 2009). HDAC inhibitors are also being studied in combination with cytotoxic or cell cycle modulating agents, monoclonal antibodies, or radiotherapy (Piekarz *et al*. 2006, 2008, Chen *et al*. 2009).

Current treatment options for malignant pheochromocytoma and paraganglioma are limited, and responses are often transient (Averbuch *et al*. 1988, Kopf *et al*. 1997, Loh *et al*. 1997, Sisson *et al*. 1999, Pacak *et al*. 2001*b*, Munver *et al*. 2003). The success of [^{131}I]MIBG, the most frequently applied therapy, depends on the drug dose and schedule used (Rose *et al*. 2003, Safford *et al*. 2003). Response rates are increased with higher doses of [^{131}I]MIBG (Fitzgerald *et al*. 2006), but higher doses are associated with greater toxicity and increased long-term risk of second malignancy (Rose *et al*. 2003, Safford *et al*. 2003).

A recent advancement is noncarrier-added high-specific activity [^{131}I]MIBG-Ultratrace Iobenguane I-131 (Ultratrace [^{131}I]MIBG, Azedra, Molecular Insight Pharmaceuticals, Inc., Cambridge, MA, USA; Coleman *et al*. 2009). This product was developed to eliminate nonradioactive MIBG, which in standard preparations competes with [^{131}I]MIBG for membrane norepinephrine transporter and perhaps vesicular transporter systems. Current clinical trials are now testing whether this reformulated agent will improve both diagnostic imaging and therapeutic efficiency (Barrett *et al*. 2010). We believe that using HDAC inhibitors together with [^{131}I]MIBG-Ultratrace Iobenguane I-131 may result in much better and perhaps therapeutically more efficient treatment with [^{131}I]MIBG for pheochromocytoma and paraganglioma tumors.

An alternative strategy to increase the efficacy of [^{131}I]MIBG treatment is to manipulate the tumor cell norepinephrine transporter system. Increased efficacy of [^{131}I]MIBG might be achieved by increasing the expression of this transporter. In this study, we demonstrated increased [^{3}H]norepinephrine uptake in MPC cells *in vitro* as well as *in vivo*. The increase was dose-dependent and found to be greatest at 72 h after treatment with either 0.5 ng/ml romidepsin or 12.5 ng/ml trichostatin A. The effects of desipramine and reserpine on the MPC cells suggest that both immediate uptake via the norepinephrine transporter and long-term retention in vesicles are responsible for the increased [^{123}I]MIBG activity in MPC cells after romidepsin and trichostatin A administration. However, other effects such as permeability of the cell membrane and osmotic activity may also play a role. Thus, the present data of an increased uptake of [^{123}I]MIBG in MPC cells after romidepsin or trichostatin A treatment support the potential use of HDAC inhibitors as 'sensitizers' to increase [^{131}I]MIBG treatment efficacy in patients with metastatic pheochromocytoma or paraganglioma. Increased uptake of both [^{18}F]fluorodopamine and [^{123}I]MIBG by liver tumors of inhibitor-treated mice compared to that observed in the liver tumors of control animals confirmed our *in vitro* findings. The increased uptake of [^{18}F]fluorodopamine did not correlate with the volume of the lesions. [^{18}F]fluorodopamine uptake in a given liver lesion, as it grows, either remained the same or decreased over time. If increased uptake of [^{18}F]fluorodopamine and [^{123}I]MIBG by liver tumors is independent of tumor size, it is most likely an effect of increased expression of the norepinephrine transporter.

For the biodistribution studies, trichostatin A was administered twice, 24 and 2 h before [^{18}F]fluorodopamine injection because of the rapid and extensive metabolism of trichostatin A. It was demonstrated that, following i.p. administration to mice (Sanderson *et al*. 2004), trichostatin A was rapidly absorbed from the peritoneum and was detectable in plasma within 6–9 min. To translate these results into clinical studies, the half-life of the HDAC inhibitors should be taken into consideration. From the present results, we conclude that romidepsin, given its recent FDA approval and longer half-life, would be more suitable for human study than trichostatin A.

Our original approach for HDAC inhibitor pretreatment was carried out using the protocol described by Goldsmith *et al*. (2007), where female athymic nude mice were treated with romidepsin at a dose of 3.6 mg/kg. Twenty-four hours following a single romidepsin injection, increased coxsackie adenovirus

receptor levels were observed, histone H3 acetylation, in athymic mice bearing human melanoma xenografts. In our experimental design, mice were given anesthesia and injection of [^{123}I]MIBG and [^{18}F]fluorodopamine, and imaged 24 h following a dose of romidepsin or trichostatin A. However, if the dose of 3.6 mg/kg as bolus was injected into mice with liver pheochromocytoma metastases, toxic effects such as tachycardia, irregular breathing, and tremor were observed and up to 30% of mice did not survive the imaging study. Thus, a single lower dose of romidepsin (2.5 mg/kg) was administered to evaluate its effect on isotope accumulation in the tumors. Mentioned toxicity from the romidepsin pretreatment *per se* could have also been as a result of increased levels of catecholamine, epinephrine, and norepinephrine. Along with [^{123}I]MIBG and [^{18}F]fluorodopamine injections, a stress response also was created when mice were handled. All these effects have been observed previously in imaging studies. Owing to extensive liver metastases and the low percentage of healthy liver parenchyma, anesthesia itself can be toxic (Martiniova *et al*. 2009*a*). [^{131}I]MIBG treatment does not require any anesthesia, and it would not be used in patients undergoing any surgical procedure that requires anesthesia.

In our *in vitro* study, there is also visible dose dependency. The FDA approved clinical doses are 14 mg/m^2 body surface administered on days 1, 8, and 15 of a 28-day cycle, and are designed for longitudinal dosing of patients. If one does the calculations for an average weight mouse ($\sim$25 g), a single standard human dose of romidepsin is 14 mg/m^2 = 14 mg $\times$1.73 m^2 body surface area (the average human male body surface area) = 24.2 mg total single dose divided by the ideal male body weight (80 kg); 24.2 mg/80 kg, the typical human dose of romidepsin is = 0.3 mg/kg per dose. If one considers that three doses are given per treatment cycle over 15 days, then the patients receive a total dose of 0.9 mg/kg. We used a single dose of 2.5 mg/kg or approximately threefold greater. In mouse studies, other investigators have used doses of romidepsin that ranged from 0.1 to 50 mg/kg. The therapeutic doses used in other animal studies were 1 and 2.5 mg/kg respectively (Hirokawa *et al*. 2005*a*,*b*, Chen *et al*. 2008).

Mice and humans often handle the same drugs very differently, so the drug dosing may be different. Therefore, for the clinical trial we are planning, the doses will be much lower with dose escalation and will be administered as infusion with more cycles than a single dose.

Our results raise the possibility of using romidepsin to increase the sensitivity of pheochromocytoma and paraganglioma lesions to [^{131}I]MIBG treatment. Future studies will focus on determining the optimal timing and dose of romidepsin. Ideally, synergy between romidepsin and [^{131}I]MIBG would allow both drugs to be used at lower concentrations than usually used as a single agent. Since romidepsin will not be used as a monotherapy, but as a sensitizer, only a few doses well below, which associates with toxic effects, will be administered before [^{131}I]MIBG treatment (Piekarz *et al*. 2006, Molife *et al*. 2007).

In summary, treatment with HDAC inhibitors increases radioisotope uptake in MPC cells *in vitro* and *in vivo* through both increased expression of the norepinephrine transporter and enhanced retention in cytoplasmic neurosecretory granules. These results suggest that HDAC inhibitors might be used to increase the response of patients with malignant pheochromocytoma and paraganglioma to [^{131}I]MIBG treatment. The same approach also could be used to increase the sensitivity of [^{131}I]MIBG scintigraphy for detecting metastatic lesions in these patients. Pretreatment with romidepsin also could be beneficial to those patients whose tumors do not take up [^{123}I]MIBG thus increasing the sensitivity of this diagnostic approach. HDAC inhibition may also help to overcome the loss of norepinephrine transporter expression that might occur with chemotherapy treatment, similar to what happens with ^{131}I treatment of thyroid cancer (Beierwaltes 1987, Simon *et al*. 2002, Gruning *et al*. 2003). Clinical studies are in progress to investigate these options.

Declaration of interest

The authors declare that there is no conflict of interest that could be perceived as prejudicing the impartiality of the research reported.

Funding

This research was supported in part by the NIH grant R01-CA48017 and a grant from the Pheo Para Alliance (to A S Tischler) and APVV-0148-06 (to R Kvetnansky). This work also was supported by the intramural program of the National Institute of Child Health and Human Development, the National Cancer Institute, the National Institute of Biomedical Imaging and Bioengineering, and the National Institute of Mental Health at the National Institutes of Health.

Acknowledgements

We thank Andrea Limpuangthip for her technical assistance and Samantha Peters for her editorial help. We thank Dr Nancy Nader for her guidance and support.

References

Adjalle R, Plouin PF, Pacak K & Lehnert H 2009 Treatment of malignant pheochromocytoma. *Hormone and Metabolic Research* **41** 687–696. (doi:10.1055/s-0029-1231025)

Averbuch SD, Steakley CS, Young RC, Gelmann EP, Goldstein DS, Stull R & Keiser HR 1988 Malignant pheochromocytoma: effective treatment with a combination of cyclophosphamide, vincristine, and dacarbazine. *Annals of Internal Medicine* **109** 267–273.

Barrett JA, Joyal JL, Hillier SM, Maresca KP, Femia FJ, Kronauge JF, Boyd M, Mairs RJ & Babich JW 2010 Comparison of high-specific-activity ultratrace $^{123/131}$I-MIBG and carrier-added $^{123/131}$I-MIBG on efficacy, pharmacokinetics, and tissue distribution. *Cancer Biotherapy & Radiopharmaceuticals* **25** 299–308. (doi:10.1089/cbr.2009.0695)

Beierwaltes WH 1987 Treatment of neuroblastoma with ^{131}I-MIBG: dosimetric problems and perspectives. *Medical and Pediatric Oncology* **15** 188–191. (doi:10.1002/mpo.2950150409)

Chen X, Gardner ER & Figg WD 2008 Determination of the cyclic depsipeptide FK228 in human and mouse plasma by liquid chromatography with mass-spectrometric detection. *Journal of Chromatography. B. Analytical Technologies in the Biomedical and Life Sciences* **865** 153–158. (doi:10.1016/j.jchromb.2008.02.015)

Chen J, Zhang M, Ju W & Waldmann TA 2009 Effective treatment of a murine model of adult T-cell leukemia using depsipeptide and its combination with unmodified daclizumab directed toward CD25. *Blood* **113** 1287–1293. (doi:10.1182/blood-2008-04-149658)

Cleary S & Phillips JK 2006 The norepinephrine transporter and pheochromocytoma. *Annals of the New York Academy of Sciences* **1073** 263–269. (doi:10.1196/annals.1353.029)

Coleman RE, Stubbs JB, Barrett JA, de la Guardia M, Lafrance N & Babich JW 2009 Radiation dosimetry, pharmacokinetics, and safety of ultratrace Iobenguane I-131 in patients with malignant pheochromocytoma/paraganglioma or metastatic carcinoid. *Cancer Biotherapy & Radiopharmaceuticals* **24** 469–475. (doi:10.1089/cbr.2008.0584)

Cornelissen J, Tytgat GA, van den Brug M, van Kuilenburg AB, Voute PA & van Gennip AH 1997 Menadione inhibits MIBG uptake in two neuroendocrine cell lines. *Journal of Neuro-Oncology* **31** 147–151. (doi:10.1023/A:1005718421774)

Eisenhofer G, Hovevey-Sion D, Kopin IJ, Miletich R, Kirk KL, Finn R & Goldstein DS 1989 Neuronal uptake and metabolism of 2- and 6-fluorodopamine: false neurotransmitters for positron emission tomographic imaging of sympathetically innervated tissues. *Journal of Pharmacology and Experimental Therapeutics* **248** 419–427.

Eldadah BA, Pacak K, Eisenhofer G, Holmes C, Kopin IJ & Goldstein DS 2004 Cardiac uptake-1 inhibition by high circulating norepinephrine levels in patients with pheochromocytoma. *Hypertension* **43** 1227–1232. (doi:10.1161/01.HYP.0000127305.87552.d6)

Fitzgerald PA, Goldsby RE, Huberty JP, Price DC, Hawkins RA, Veatch JJ, Dela Cruz F, Jahan TM, Linker CA, Damon L *et al.* 2006 Malignant pheochromocytomas and paragangliomas: a phase II study of therapy with high-dose ^{131}I-metaiodobenzylguanidine (^{131}I-MIBG). *Annals of the New York Academy of Sciences* **1073** 465–490. (doi:10.1196/annals.1353.050)

Furuya F, Shimura H, Suzuki H, Taki K, Ohta K, Haraguchi K, Onaya T, Endo T & Kobayashi T 2004 Histone deacetylase inhibitors restore radioiodide uptake and retention in poorly differentiated and anaplastic thyroid cancer cells by expression of the sodium/iodide symporter thyroperoxidase and thyroglobulin. *Endocrinology* **145** 2865–2875. (doi:10.1210/en.2003-1258)

Gaal J, Burnichon N, Korpershoek E, Roncelin I, Bertherat J, Plouin PF, de Krijger RR, Gimenez-Roqueplo AP & Dinjens WN 2010 Isocitrate dehydrogenase mutations are rare in pheochromocytomas and paragangliomas. *Journal of Clinical Endocrinology and Metabolism* **95** 1274–1278. (doi:10.1210/jc.2009-2170)

Glowniak JV, Kilty JE, Amara SG, Hoffman BJ & Turner FE 1993 Evaluation of metaiodobenzylguanidine uptake by the norepinephrine, dopamine and serotonin transporters. *Journal of Nuclear Medicine* **34** 1140–1146.

Goldsmith ME, Aguila A, Steadman K, Martinez A, Steinberg SM, Alley MC, Waud WR, Bates SE & Fojo T 2007 The histone deacetylase inhibitor FK228 given prior to adenovirus infection can boost infection in melanoma xenograft model systems. *Molecular Cancer Therapeutics* **6** 496–505. (doi:10.1158/1535-7163.MCT-06-0431)

Gonias S, Goldsby R, Matthay KK, Hawkins R, Price D, Huberty J, Damon L, Linker C, Sznewajs A, Shiboski S *et al.* 2009 Phase II study of high-dose [^{131}I]metaiodobenzylguanidine therapy for patients with metastatic pheochromocytoma and paraganglioma. *Journal of Clinical Oncology* **27** 4162–4168. (doi:10.1200/JCO.2008.21.3496)

Green MV, Seidel J, Vaquero JJ, Jagoda E, Lee I & Eckelman WC 2001 High resolution PET, SPECT and projection imaging in small animals. *Computerized Medical Imaging and Graphics* **25** 79–86. (doi:10.1016/S0895-6111(00)00057-4)

Gruning T, Tiepolt C, Zophel K, Bredow J, Kropp J & Franke WG 2003 Retinoic acid for redifferentiation of thyroid cancer – does it hold its promise? *European Journal of Endocrinology* **148** 395–402. (doi:10.1530/eje.0.1480395)

Hirokawa Y, Arnold M, Nakajima H, Zalcberg J & Maruta H 2005*a* Signal therapy of breast cancers by the HDAC inhibitor FK228 that blocks the activation of PAK1 and abrogates the tamoxifen-resistance. *Cancer Biology & Therapy* **4** 956–960. (doi:10.4161/cbt.4.9.1911)

Hirokawa Y, Nakajima H, Hanemann CO, Kurtz A, Frahm S, Mautner V & Maruta H 2005*b* Signal therapy of NF1-deficient tumor xenograft in mice by the anti-PAK1 drug FK228. *Cancer Biology & Therapy* **4** 379–381. (doi:10.4161/cbt.4.4.1649)

Huang H, Abraham J, Hung E, Averbuch S, Merino M, Steinberg SM, Pacak K & Fojo T 2008 Treatment of malignant pheochromocytoma/paraganglioma with cyclophosphamide, vincristine, and dacarbazine: recommendation from a 22-year follow-up of 18 patients. *Cancer* **113** 2020–2028. (doi:10.1002/cncr.23812)

Hutchins GD, Miller MA, Soon VC & Receveur T 2008 Small animal PET imaging. *Institute of Laboratory Animal Resources Journal* **49** 54–65.

Ichijo T, Voutetakis A, Cotrim AP, Bhattachryya N, Fujii M, Chrousos GP & Kino T 2005 The Smad6-histone deacetylase 3 complex silences the transcriptional activity of the glucocorticoid receptor: potential clinical implications. *Journal of Biological Chemistry* **280** 42067–42077. (doi:10.1074/jbc.M509338200)

Jaques S Jr, Tobes MC, Sisson JC, Baker JA & Wieland DM 1984 Comparison of the sodium dependency of uptake of meta-Iodobenzylguanidine and norepinephrine into cultured bovine adrenomedullary cells. *Molecular Pharmacology* **26** 539–546.

John H, Ziegler WH, Hauri D & Jaeger P 1999 Pheochromocytomas: can malignant potential be predicted? *Urology* **53** 679–683. (doi:10.1016/S0090-4295(98)00612-8)

Keyes JW Jr 1995 SUV: standard uptake or silly useless value? *Journal of Nuclear Medicine* **36** 1836–1839.

Kim MS, Blake M, Baek JH, Kohlhagen G, Pommier Y & Carrier F 2003 Inhibition of histone deacetylase increases cytotoxicity to anticancer drugs targeting DNA. *Cancer Research* **63** 7291–7300.

Kitazono M, Robey R, Zhan Z, Sarlis NJ, Skarulis MC, Aikou T, Bates S & Fojo T 2001 Low concentrations of the histone deacetylase inhibitor, depsipeptide (FR901228), increase expression of the Na(+)/I(−) symporter and iodine accumulation in poorly differentiated thyroid carcinoma cells. *Journal of Clinical Endocrinology and Metabolism* **86** 3430–3435. (doi:10.1210/jc.86.7.3430)

Kolby L, Bernhardt P, Levin-Jakobsen AM, Johanson V, Wangberg B, Ahlman H, Forssell-Aronsson E & Nilsson O 2003 Uptake of meta-iodobenzylguanidine in neuroendocrine tumours is mediated by vesicular monoamine transporters. *British Journal of Cancer* **89** 1383–1388. (doi:10.1038/sj.bjc.6601276)

Kopf D, Bockisch A, Steinert H, Hahn K, Beyer J, Neumann HP, Hensen J & Lehnert H 1997 Octreotide scintigraphy and catecholamine response to an octreotide challenge in malignant phaeochromocytoma. *Clinical Endocrinology* **46** 39–44. (doi:10.1046/j.1365-2265.1997.d01-1738.x)

Kumar A, Choi KH, Renthal W, Tsankova NM, Theobald DE, Truong HT, Russo SJ, Laplant Q, Sasaki TS, Whistler KN *et al.* 2005 Chromatin remodeling is a key mechanism underlying cocaine-induced plasticity in striatum. *Neuron* **48** 303–314. (doi:10.1016/j.neuron.2005.09.023)

Lenders JW, Eisenhofer G, Mannelli M & Pacak K 2005 Phaeochromocytoma. *Lancet* **366** 665–675. (doi:10.1016/S0140-6736(05)67139-5)

Li QY, Jones PL, Lafferty RP, Safer D & Levy RJ 2002 Thymosin beta4 regulation, expression and function in aortic valve interstitial cells. *Journal of Heart Valve Disease* **11** 726–735.

Lingen B, Bruss M & Bonisch H 1994 Cloning and expression of the bovine sodium- and chloride-dependent noradrenaline transporter. *FEBS Letters* **342** 235–238. (doi:10.1016/0014-5793(94)80508-3)

Loh KC, Fitzgerald PA, Matthay KK, Yeo PP & Price DC 1997 The treatment of malignant pheochromocytoma with iodine-131 metaiodobenzylguanidine (^{131}I-MIBG): a comprehensive review of 116 reported patients. *Journal of Endocrinological Investigation* **20** 648–658.

Mann BS, Johnson JR, Cohen MH, Justice R & Pazdur R 2007 FDA approval summary: vorinostat for treatment of advanced primary cutaneous T-cell lymphoma. *Oncologist* **12** 1247–1252. (doi:10.1634/theoncologist.12-10-1247)

Marks PA, Richon VM & Rifkind RA 2000 Histone deacetylase inhibitors: inducers of differentiation or apoptosis of transformed cells. *Journal of the National Cancer Institute* **92** 1210–1216. (doi:10.1093/jnci/92.15.1210)

Marks P, Rifkind RA, Richon VM, Breslow R, Miller T & Kelly WK 2001 Histone deacetylases and cancer: causes and therapies. *Nature Reviews. Cancer* **1** 194–202. (doi:10.1038/35106079)

Martiniova L, Kotys MS, Thomasson D, Schimel D, Lai EW, Bernardo M, Merino MJ, Powers JF, Ruzicka J, Kvetnansky R *et al.* 2009*a* Noninvasive monitoring of a murine model of metastatic pheochromocytoma: a comparison of contrast-enhanced microCT and none-nhanced MRI. *Journal of Magnetic Resonance Imaging* **29** 685–691. (doi:10.1002/jmri.21654)

Martiniova L, Lai EW, Elkahloun AG, Abu-Asab M, Wickremasinghe A, Solis DC, Perera SM, Huynh TT, Lubensky IA, Tischler AS *et al.* 2009*b* Characterization of an animal model of aggressive metastatic pheochromocytoma linked to a specific gene signature. *Clinical & Experimental Metastasis* **26** 239–250. (doi:10.1007/s10585-009-9236-0)

Molife R, Fong P, Scurr M, Judson I, Kaye S & de Bono J 2007 HDAC inhibitors and cardiac safety. *Clinical Cancer Research* **13** 1068 (author reply 1068–1069). (doi:10.1158/1078-0432.CCR-06-1715)

Mundschenk J & Lehnert H 1998 Malignant pheochromocytoma. *Experimental and Clinical Endocrinology & Diabetes* **106** 373–376. (doi:10.1055/s-0029-1212001)

Munver R, Del Pizzo JJ & Sosa RE 2003 Adrenal-preserving minimally invasive surgery: the role of laparoscopic partial adrenalectomy, cryosurgery, and radiofrequency ablation of the adrenal gland. *Current Urology Reports* **4** 87–92. (doi:10.1007/s11934-003-0065-4)

Nomura K, Kimura H, Shimizu S, Kodama H, Okamoto T, Obara T & Takano K 2009 Survival of patients with metastatic malignant pheochromocytoma and efficacy of combined cyclophosphamide, vincristine, and dacarbazine chemotherapy. *Journal of Clinical Endocrinology and Metabolism* **94** 2850–2856. (doi:10.1210/jc.2008-2697)

Ohta S, Lai EW, Morris JC, Pang AL, Watanabe M, Yazawa H, Zhang R, Green JE, Chan WY, Sirajuddin P *et al.* 2008 Metastasis-associated gene expression profile of liver and subcutaneous lesions derived from mouse pheochromocytoma cells. *Molecular Carcinogenesis* **47** 245–251. (doi:10.1002/mc.20388)

O'Riordain DS, Young WF Jr, Grant CS, Carney JA & van Heerden JA 1996 Clinical spectrum and outcome of functional extraadrenal paraganglioma. *World Journal of Surgery* **20** 916–921. (doi:10.1007/s002689900139)

Pacak K, Chrousos GP, Koch CA, Lenders JW & Eisenhofer G 2001*a* Pheochromocytoma: progress in diagnosis, therapy, and genetics. In *Adrenal Disorders*, 1st edn, pp 479–523. Eds A Margioris & GP Chrousos. Totowa: Humana Press.

Pacak K, Linehan WM, Eisenhofer G, Walther MM & Goldstein DS 2001*b* Recent advances in genetics, diagnosis, localization, and treatment of pheochromocytoma. *Annals of Internal Medicine* **134** 315–329.

Piekarz RL, Frye AR, Wright JJ, Steinberg SM, Liewehr DJ, Rosing DR, Sachdev V, Fojo T & Bates SE 2006 Cardiac studies in patients treated with depsipeptide, FK228, in a phase II trial for T-cell lymphoma. *Clinical Cancer Research* **12** 3762–3773. (doi:10.1158/1078-0432.CCR-05-2095)

Piekarz R, Luchenko V, Draper D, Wright J, Figg W, Fojo A & Bates S 2008 Phase I trial of romidepsin, a histone deacetylase inhibitor, given on days one, three and five in patients with thyroid and other advanced cancers. *Journal of Clinical Oncology* **26** abstr 3571.

Piekarz RL, Frye R, Turner M, Wright JJ, Allen SL, Kirschbaum MH, Zain J, Prince HM, Leonard JP, Geskin LJ *et al.* 2009 Phase II multi-institutional trial of the histone deacetylase inhibitor romidepsin as monotherapy for patients with cutaneous T-cell lymphoma. *Journal of Clinical Oncology* **27** 5410–5417. (doi:10.1200/JCO.2008.21.6150)

Plouin PF, Gimenez-Roqueplo AP, La Batide Alanore A, Salenave S & Duclos JM 2000 Recent progress in the diagnosis, prognostic evaluation and treatment of pheochromocytomas. *La Revue de Medecine Interne* **21** 1075–1085. (doi:10.1016/S0248-8663(00)00268-X)

Powers JF, Evinger MJ, Tsokas P, Bedri S, Alroy J, Shahsavari M & Tischler AS 2000 Pheochromocytoma cell lines from heterozygous neurofibromatosis knockout mice. *Cell and Tissue Research* **302** 309–320. (doi:10.1007/s004410000290)

Rose B, Matthay KK, Price D, Huberty J, Klencke B, Norton JA & Fitzgerald PA 2003 High-dose ^{131}I-metaiodobenzylguanidine therapy for 12 patients with malignant pheochromocytoma. *Cancer* **98** 239–248. (doi:10.1002/cncr.11518)

Safford SD, Coleman RE, Gockerman JP, Moore J, Feldman JM, Leight GS Jr, Tyler DS & Olson JA Jr 2003 Iodine -131 metaiodobenzylguanidine is an effective treatment for malignant pheochromocytoma and paraganglioma. *Surgery* **134** 956–962 (discussion 962–963). (doi:10.1016/S0039-6060(03)00426-4)

Sanderson L, Taylor GW, Aboagye EO, Alao JP, Latigo JR, Coombes RC & Vigushin DM 2004 Plasma pharmacokinetics and metabolism of the histone deacetylase inhibitor trichostatin a after intraperitoneal administration to mice. *Drug Metabolism and Disposition* **32** 1132–1138. (doi:10.1124/dmd.104.000638)

Sandor V, Robbins AR, Robey R, Myers T, Sausville E, Bates SE & Sackett DL 2000*a* FR901228 causes mitotic arrest but does not alter microtubule polymerization. *Anticancer Drugs* **11** 445–454. (doi:10.1097/00001813-200007000-00005)

Sandor V, Senderowicz A, Mertins S, Sackett D, Sausville E, Blagosklonny MV & Bates SE 2000*b* P21-dependent g(1)arrest with downregulation of cyclin D1 and upregulation of cyclin E by the histone deacetylase inhibitor FR901228. *British Journal of Cancer* **83** 817–825. (doi:10.1054/bjoc.2000.1327)

Seidel J 2003 Resolution uniformity and sensitivity of the NIH ATLAS small animal PET scanner: comparison to simulated LSO scanners without depth-of-interaction capability. *IEEE Transactions on Nuclear Science* **50** 1347–1350. (doi:10.1109/TNS.2003.817282)

Shilkrut M, Bar-Deroma R, Bar-Sela G, Berniger A & Kuten A 2010 Low-dose iodine-131 metaiodobenzylguanidine therapy for patients with malignant pheochromocytoma and paraganglioma: single center experience. *American Journal of Clinical Oncology* **33** 79–82. (doi:10.1097/COC.0b013e31819e2c28)

Simon D, Korber C, Krausch M, Segering J, Groth P, Gorges R, Grunwald F, Muller-Gartner HW, Schmutzler C, Kohrle J *et al.* 2002 Clinical impact of retinoids in redifferentiation therapy of advanced thyroid cancer: final results of a pilot study. *European Journal of Nuclear Medicine and Molecular Imaging* **29** 775–782. (doi:10.1007/s00259-001-0737-6)

Sisson JC & Wieland DM 1986 Radiolabeled metaiodobenzylguanidine: pharmacology and clinical studies. *American Journal of Physiologic Imaging* **1** 96–103.

Sisson JC, Shapiro B, Meyers L, Mallette S, Mangner TJ, Wieland DM, Glowniak JV, Sherman P & Beierwaltes

WH 1987 Metaiodobenzylguanidine to map scintigraphically the adrenergic nervous system in man. *Journal of Nuclear Medicine* **28** 1625–1636.

Sisson JC, Shapiro B, Shulkin BL, Urba S, Zempel S & Spaulding S 1999 Treatment of malignant pheochromocytomas with 131-I metaiodobenzylguanidine and chemotherapy. *American Journal of Clinical Oncology* **22** 364–370. (doi:10.1097/00000421-199908000-00008)

Takahashi K, Ashizawa N, Minami T, Suzuki S, Sakamoto I, Hayashi K, Tomiyasu S, Sumikawa K, Kitamura K, Eto T *et al.* 1999 Malignant pheochromocytoma with multiple hepatic metastases treated by chemotherapy and transcatheter arterial embolization. *Internal Medicine* **38** 349–354. (doi:10.2169/internalmedicine.38.349)

Toyama H, Ichise M, Liow JS, Modell KJ, Vines DC, Esaki T, Cook M, Seidel J, Sokoloff L, Green MV *et al.* 2004 Absolute quantification of regional cerebral glucose utilization in mice by ^{18}F-FDG small animal PET scanning and 2-14C-DG autoradiography. *Journal of Nuclear Medicine* **45** 1398–1405.

Ueda H, Manda T, Matsumoto S, Mukumoto S, Nishigaki F, Kawamura I & Shimomura K 1994*a* FR901228, a novel antitumor bicyclic depsipeptide produced by *Chromobacterium violaceum* No. 968. III. Antitumor activities on experimental tumors in mice. *Journal of Antibiotics* **47** 315–323.

Ueda H, Nakajima H, Hori Y, Fujita T, Nishimura M, Goto T & Okuhara M 1994*b* FR901228, a novel antitumor bicyclic depsipeptide produced by *Chromobacterium violaceum* No. 968. I. Taxonomy, fermentation, isolation, physico-chemical and biological properties, and antitumor activity. *Journal of Antibiotics* **47** 301–310.

Van Lint C, Emiliani S & Verdin E 1996 The expression of a small fraction of cellular genes is changed in response to histone hyperacetylation. *Gene Expression* **5** 245–253.